

Further results on the in situ anaerobic corrosion of carbon steel and copper in compacted bentonite exposed to natural Opalinus Clay porewater containing native microbial populations

B. Reddy¹, C. Padovani¹, N.R. Smart¹, A.P Rance¹, A. Cook¹, A. Milodowski², L. Field², S. Kemp², N. Diomidis³

¹ Jacobs, HQ Building, Thomson Avenue, Harwell Campus, OX11 0GD, United Kingdom.

² British Geological Survey, Nicker Hill, Keyworth, Nottingham, NG12 5GG

³ Nagra, Hardstrasse 73, Postfach 280, 5430 Wettingen, Switzerland

Corresponding author: nikitas.diomidis@nagra.ch

Since 2012, a long-term in situ corrosion experiment (IC-A) is being conducted in the Mont Terri Underground Research Laboratory in Switzerland to investigate the corrosion behaviour of candidate canister materials in conditions representative of the Swiss concept for the disposal of high-level waste and spent nuclear fuel. To date, carbon steel and various types of copper coatings have been retrieved after different exposure periods of up to three years, and characterized to establish the composition of the corrosion product, the morphology of the corroded surface, the nature of the interaction between the metal and the surrounding bentonite, and the microbial populations in the bentonite and surrounding porewater. For carbon steel specimens, a complex corrosion product was identified, consisting predominantly of magnetite. Much less alteration on either the metal or the bentonite was observed in the case of copper samples. Low average anaerobic corrosion rates were measured for carbon steel and a very modest amount of alteration was identified on copper. The density and the initial form of the

bentonite had a small influence on the rate of corrosion, across all materials. This paper summarises the results of the experimental programme obtained to date and discusses the relationship observed between exposure time and the evolution of the metal-bentonite interface for both carbon steel and copper.

Keywords: Copper, carbon steel, anaerobic, corrosion, microbial, bentonite, radioactive waste

1 Introduction

Nagra (National Cooperative for the Disposal of Radioactive Waste, Switzerland) is considering using carbon steel as a potential canister material for disposal of high-level waste (HLW) and spent fuel (SF) in a geological disposal facility constructed in the Opalinus Clay host rock [1]. An alternative canister design consists of carbon steel containers coated with a thin copper layer [2], similar to the Canadian used fuel container [3]. In either disposal concept, compacted bentonite clay will be placed around the disposal canisters since it is expected to provide a favourable chemical and hydromechanical environment for preserving its integrity for long periods of time after emplacement in the host rock. After canister breaching, the bentonite is also expected to provide other beneficial functions, including a strong retention capability for any radionuclides that are released during contact of the waste with the groundwater and the prevention of any hydraulic short-cuts developing between the canisters and the excavation damaged zones of the drifts [4].

With canister lifetime requirements generally in the range of several thousand or tens of thousands of years, robust lifetime predictions require dependable corrosion data for conditions representative of those expected during disposal. In order to closely mimic disposal conditions one would have to perform experiments in the host rock that has been selected for the construction of the repository, typically in an underground research laboratory [5]. Several in situ corrosion experiments have been performed over the years in support of various national radioactive waste disposal concepts [6-17].

Since 2012, an in situ corrosion experiment is being carried out at the Mont Terri underground rock laboratory (URL) in Switzerland with an overall long-term objective to study the corrosion behaviour of candidate disposal canister materials under simulated repository conditions, i.e. under anaerobic conditions in bentonite saturated with Opalinus Clay porewater.

Previous results have been presented in [14, 18], while the evolution of microbial populations in bentonite and porewater, and the evolution of porewater composition are reported in [19]. This paper focuses on the long-term corrosion of the container materials, and the corrosion products produced.

2 Experimental

2.1 Corrosion coupons

A carbon steel partial canister prototype with an electron beam welded lid was manufactured by TWI (The Welding Institute, UK). The grade of the steel was ASTM A694-08 F65 (composition, wt-%: C 0.11; Mn 1.3; Si: 0.20; P 0.010; Si 0.002; Cr: 0.10; Ni 0.07; Mo 0.17; V 0.053; Nb 0.037; Fe bal.). A reduced pressure electron-beam welding process was used (5×10^{-2} mbar pressure, helium overpressure, accelerating voltage 150 kV, maximum beam current 255 mA, welding speed at full current 80 mm min^{-1}) to perform a full penetration 14 cm deep weld. A post-weld heat treatment (600°C for 4 then air-cooled) was subsequently applied before the material was used to prepare the test coupons. During this process the cylinder (base metal) and the weld region were heat-treated and cut into sections, which were then used as the starting material for manufacture of corrosion coupons. The details of the manufacture of the carbon steel specimens are given in reference [18].

Electrodeposited copper (Nanovate TM C4010) [20] and cold-sprayed copper [21] coupons were provided by NWMO (Nuclear Waste Management Organisation, Canada).

All coupons were ultrasonically cleaned in acetone, then grit blasted with grade 120/220 aluminium oxide powder to achieve a consistent surface roughness, R_a , of $\sim 0.5 \mu\text{m}$ (measured using a Talysurf instrument on a representative 10% of samples). Once the coupons had been grit blasted, further ultrasonic cleaning in methanol was carried out and the coupons were weighed twice to a precision of 0.00001g. Photographs of the initial state of each specimen were taken.

2.2 Bentonite

Volclay MX-80 bentonite from Wyoming, U.S. (Amcol Specialty Minerals, U.K.), was used throughout the experiment. Two different forms of bentonite were used, as follows:

- Compacted blocks with a final nominal dry density of 1450 kg m^{-3} and 1550 kg m^{-3} . The compacted bentonite blocks were provided by Clay Technology Sweden. The bentonite was prepared to give a 95-99% degree of saturation using deionized water. The bentonite was placed into a 100 mm diameter mould that incorporated recesses for the corrosion coupons and subsequently manufactured through compaction. The compaction of the blocks was performed under vacuum and all further handling and storage performed under nitrogen.
- A mixture of pellets and powder with a final nominal dry density of 1450 kg m^{-3} . In this case, bentonite pellets and powder were combined in a specified mass and to specified volume to obtain the nominal (dry) density.

2.3 Assembly and emplacement of corrosion test modules

The design of the corrosion modules used in the experiment, their manufacture and emplacement in the testing borehole is described in previous work [18]. A brief summary of key points is provided below to facilitate interpretation of the content of this work.

The modules were assembled in an argon-filled glovebox ($<0.1 \text{ ppm}$ oxygen), to ensure that the starting conditions for the experiments were anoxic. Each module contained 4 layers of 3 corrosion coupons each (3 coupons per material and module).

Before transport to the test site, modules containing compacted bentonite blocks were pre-saturated in the glovebox by submerging them in anoxic artificial groundwater for two days, while the bentonite modules made starting from pellets were soaked for ten days. After soaking, each module was placed in a sealed transfer vessel inside an argon-purged glovebox to retain an anoxic atmosphere during transport to the underground laboratory at Mont Terri, Switzerland. The modules were emplaced in the borehole on 30 September 2014. The testing borehole water pressure was $\sim 10 \text{ bar}$ and the ambient temperature was $\sim 14 \text{ }^\circ\text{C}$.

2.4 Retrieval and dismantling of test modules

The test modules were removed for analysis on July 4, 2017 after ~1008 days exposure, and transported for analysis inside argon-purged, sealed transport containers. They were dismantled in a glovebox under anoxic conditions to prevent any aerobic corrosion reactions ~1024 days after emplacement. Dismantling was performed in a pre-cleaned and pre-sterilized, argon-purged glovebox.

2.5 Analysis of corrosion coupons

The corrosion coupons and selected samples of bentonite were removed and prepared for analysis inside the argon glovebox. Post-mortem characterisation was carried out at the Oxford University Materials Service. Samples for characterisation were shipped inside airtight containers sealed under argon. The materials were stored inside such containers up to just before the analysis, thus minimising any potential interaction with air. In the case of Raman spectroscopy, the analysis was carried out directly on sealed samples through a laser-transparent glass window without exposure to air. The following types of analysis were carried out:

- SEM examination and EDX analysis was carried out using a Hitachi TM3000 SEM equipped with a Bruker X-ray analysis system.
- Raman spectroscopy used a Horiba JY LabRam Aramis confocal Raman microscope, with an exciting laser wavelength of 532 nm.
- X-ray photoelectron spectroscopy (XPS) was carried out using a Thermo Scientific K-Alpha XPS instrument equipped with a micro focussed monochromated Al X-ray source. The source was operated at 12 keV and a 400 micron spot size was used. The analyser operates at a constant analyser energy (CAE) of 200 eV for wide binding energy survey scans and at 50 eV for detailed scans. Charge neutralization was applied using a combined low energy / ion flood source.

Weight loss measurements were carried out according to ASTM G1 [22]. Clarke's solution (inhibited hydrochloric acid) and 50% hydrochloric acid were used as the descaling agent for carbon steel coupons and copper coupons respectively. For carbon steel coupons only two exposures were carried out (i.e. the first exposure was sufficient to remove all the corrosion product, the second was used to correct the first to take into account the corrosion rate of the bare metal in the inhibited acid). For copper coupons the process was repeated until a clear change in slope of the weight loss graph (i.e. weight loss vs. number of descaling steps) could be determined, indicating that all the corrosion product had been removed [23].

The weight loss was converted into an 'average' corrosion rate given in units of $\mu\text{m yr}^{-1}$ [22]. This average reflects both a geometric average (the value obtained if all the surface corroded uniformly) and a time average (the value obtained if the surface corroded at the same rate throughout the experimental duration). Profilometry of the coupons was carried out after the weight loss measurements to evaluate the surface topography of the metal. These tests were carried out using a confocal laser scanning microscope (Keyence VK-X200). An area ($\sim 3.3 \times 4.5$ mm) on one flat side of the coupons was mapped through the acquisition and stitching of 49 separate maps, with a vertical resolution of 0.5 μm . Roughness parameters were calculated for ten individual line profiles across these maps in both the horizontal and vertical directions. For comparison, measurements on pristine samples (i.e. coupons which had not been exposed) were also taken.

2.6 Analysis of bentonite

A visually 'unaltered' bentonite sample, extracted in an area distant from the corroded coupons, was taken from the bentonite block and used as baseline for comparison with samples taken immediately adjacent to the corroding coupons. In the case of carbon steel coupons, this region was characterised by a narrow zone of iron-stained bentonite between 2 to 4 mm wide. The methodology and approach used were similar to that used previously to study samples from iron-bentonite interaction experiments [18].

Polished thin sections were prepared from bentonite sub-samples by impregnation in epoxy resin under vacuum and polished with propanol and 0.45 μm diamond paste. Low magnification images of whole thin sections were recorded by digitally scanning the thin section using an Epsom Perfection 1240U flatbed scanner equipped with a transmitted light (transparency) scanning attachment. Sub-samples were then initially examined using a Zeiss Axioplan 2 optical petrographic (polarising) microscope. Detailed examination was done using BSEM, EDXA and energy-dispersive electron probe microanalysis (EPMA) using a FEI Company QUANTA 600 environmental SEM in conjunction with INCA Microanalysis software.

In order to study the bulk mineralogy of the samples and to prevent further oxidation of any Fe-bearing species, ~10 mg portions of material were rapidly removed using a scalpel and ground to a fine powder. The powder was then deposited onto the surface of 'zero-background' silicon crystal substrate XRD mounts using a single drop of acetone to form a deposit with random crystal orientation. The preparation of oriented mounts involved dispersing ~10 mg portions of material in deionised water using ultrasound treatment without dispersant. The dispersions were then pipetted onto glass slip substrates and allowed to dry at room temperature.

XRD analysis was carried out using a PANalytical X'Pert Pro series diffractometer equipped with a cobalt-target tube, X'Celerator detector and operated at 45 kV and 40 mA. The random powder mounts were scanned from 4.5-85 °2 θ at 2.06 °2 θ min⁻¹. Diffraction data were initially analysed using PANalytical X'Pert HighScore Plus version 4.1 software coupled to the latest version of the International Centre for Diffraction Data database. The basal XRD spacings of smectite-group minerals are particularly susceptible to the prevailing humidity and temperature conditions when analysed. Therefore, in order to ensure constant conditions, air-dried oriented glass slip mounts were placed in an Anton Parr THC (controlled temperature and humidity) chamber attached to the diffractometer system and operated at 50% relative humidity and 40 °C.

3 Results

3.1 Surface characterisation of metal coupons

Optical observations of the coupons are shown in Figure 1 Optical images of metal coupons before and after exposure, and adjacent bentonite after exposure. The samples showed variable colouration suggesting a heterogeneous surface. In places there were signs of adhering bentonite and/or alteration phases on the surfaces of the corrosion coupons. In other cases, the samples of bentonite in contact with the metal samples showed adhering phases suggesting that, upon mechanical disassembly, alteration products remained either attached to the metal coupons or to the bentonite. The colouration seen on carbon steel coupons was typically dark grey, while on copper it was typical of metallic copper. The bentonite surrounding the carbon steel coupons exhibited black staining at the interface with the coupon, with a brown discolouration penetrating ~2 mm into the bentonite from interface. The bentonite surrounding the copper samples showed no development of colouration, although some dark grey and whitish discolouration was visible at the interface. Overall, there was less bentonite adherent on copper than on steel.

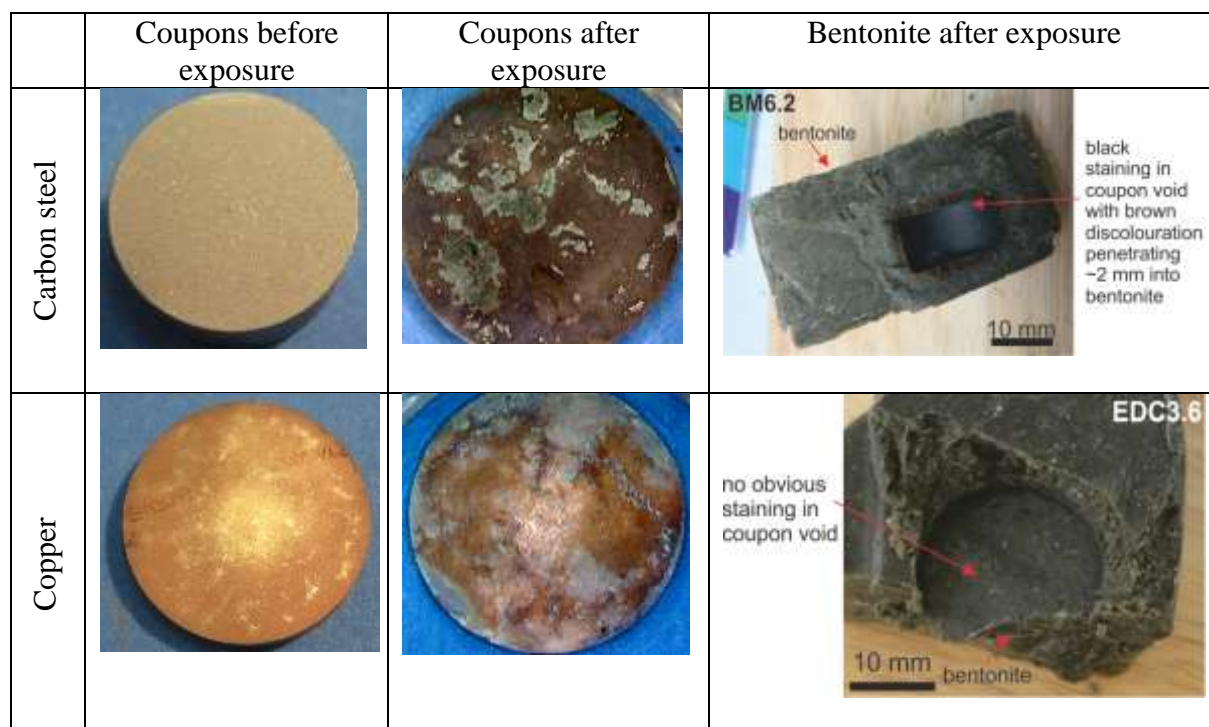


Figure 1 Optical images of metal coupons before and after exposure, and adjacent bentonite after exposure.

SEM examination was carried out on a selection of copper and carbon steel samples removed from the modules. Examples of representative micrographs and EDX analyses are given in Figure 2 and 3 for steel and copper respectively. The surface of the samples appears to have regions covered with adherent bentonite and regions where the metal is exposed. This was confirmed by EDX spot analysis (not shown). There were no significant differences between the elemental composition obtained on same type of metal coupons from different modules.

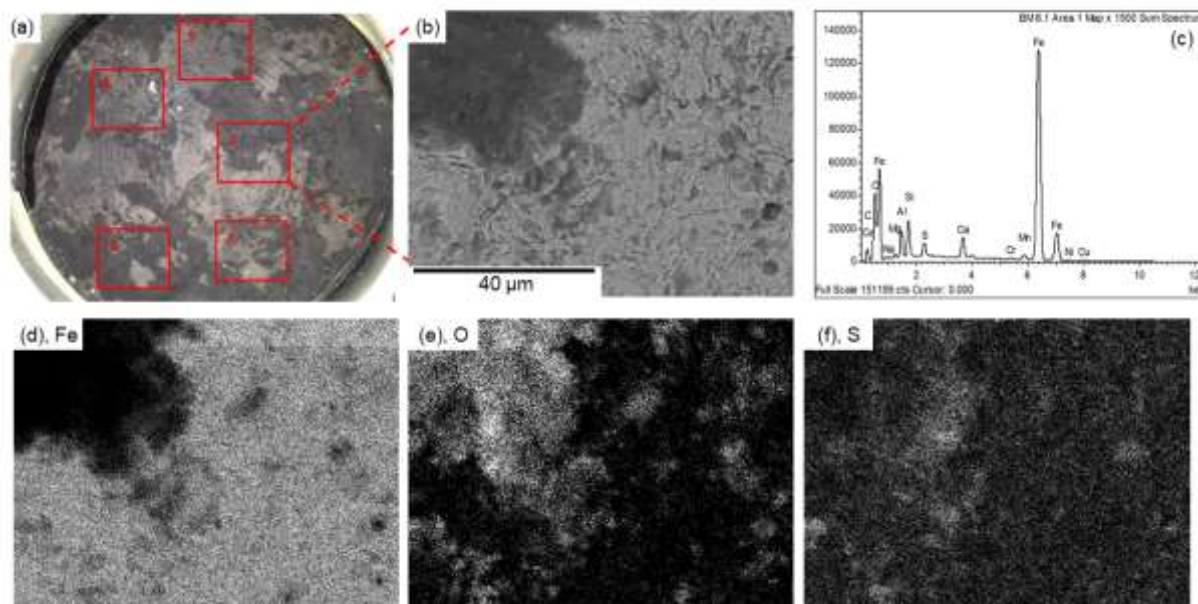


Figure 2. SEM-EDX analysis of base metal carbon steel after in situ exposure for 1024 days in bentonite pellets. (a) optical image of coupon, with analysis areas marked. (b) backscattered electron image of area 1 shown in in (a), (c) overall EDX spectrum of (b). (d-f) elemental maps acquired from area (b).

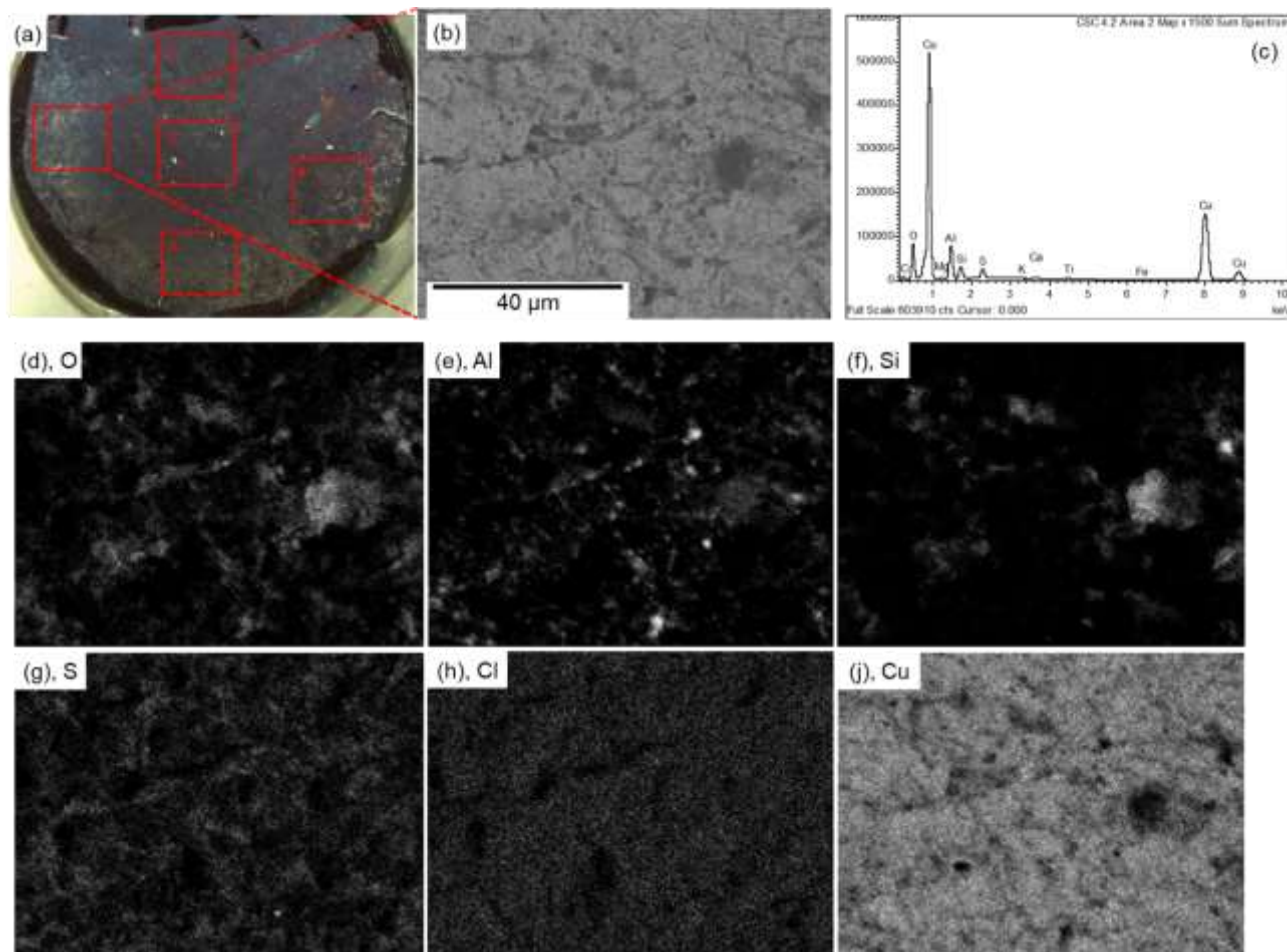


Figure 3. SEM-EDX analysis of cold-sprayed copper coupon after in situ exposure for 1024 days in bentonite pellets. (a) optical image of coupon, with analysis areas marked. (b) backscattered electron image of area 2 shown in (a). (c) overall EDX spectrum of (b). (d-j) elemental maps acquired from area (b).

Raman spectra obtained from three areas on a carbon steel base metal coupon, and from three areas of an electrodeposited copper coupon are shown in Figure 4. All spectra have exhibited fluorescence originating from the adhering bentonite making peak identification difficult. For the carbon steel base metal coupon, a peak was observed at $\sim 300\text{ cm}^{-1}$. Reference spectra show that Raman peaks corresponding to haematite are observed at $290\text{--}300\text{ cm}^{-1}$ [24] and that Raman peaks corresponding to magnetite are observed at 310 cm^{-1} , $660\text{--}670\text{ cm}^{-1}$, 700 cm^{-1} and $1400\text{--}1600\text{ cm}^{-1}$ [24, 25], thus suggesting iron oxide species were formed. For the copper

coupon (electrodeposited copper), Raman peaks were seen at $\sim 110\text{ cm}^{-1}$, $\sim 300\text{ cm}^{-1}$ and 1600 cm^{-1} . Reference spectra [26] show that the peaks present at $\sim 300\text{ cm}^{-1}$ may be associated with CuO and that the peaks in the region of $100\text{-}200\text{ cm}^{-1}$ may attributed to Cu_2O .

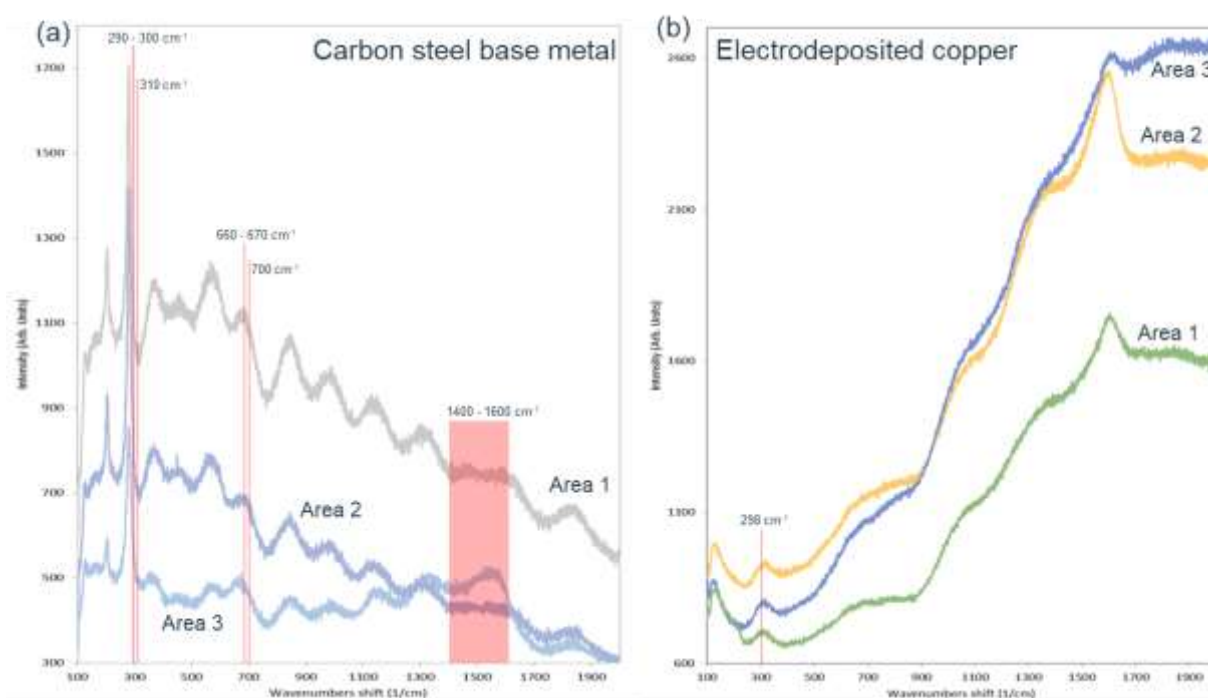


Figure 4. Raman spectra from carbon steel base metal weld metal coupon (a) and electrodeposited copper coupon (b). Areas 1, 2 and 3 are arbitrary points on the surface.

Table 1 presents the surface elemental concentrations obtained by XPS analysis from three points for a carbon steel coupon. The last point (Point 3) was also analysed after ion bombardment to obtain data at different depths. The following observations can be made on the basis of the analysis:

- There was generally a high level of carbon and oxygen seen at the surface of the carbon steel at the three points analysed. The carbon signal, however, decreased after ion bombardment suggesting that at least a portion of the measured carbon is adventitious.

- A number of species likely to be present in the bentonite (Na, Ca, Mg, Al and Si) or that may have arisen from the grit blasting processes used to prepare the surfaces of the metal (Al) were present in relatively significant quantities on the surfaces, indicating the presence of some bentonite and, possibly, grit blasting residues.
- The iron signal indicates that corrosion products or the metal substrate were detected, with the signal increasing from 10-15 at.% initially to 25 at.% after ion bombardment. The Fe:O ratio measured after ion bombardment to a depth of 3.3 nm was 0.4:1, compared to 0.75:1 for magnetite (Fe_3O_4) and 0.66:1 for haematite (Fe_2O_3). This lower Fe:O ratio suggests an additional source of O. Deconvolution of the XPS peak indicated that approximately 92 at.% of the O was in the form of silicate and 8 at.% in the form of iron oxide, with the amount of O in the form of silicates decreasing to 40 at.% after ion bombardment. Deconvolution of the iron peak before ion bombardment indicated 54 at.% as Fe^{3+} , 42 at.% as Fe^{2+} ($\text{Fe}^{3+} / \text{Fe}^{2+} = 1.3$) and 4 at.% as FeS_2 , after ion bombardment the $\text{Fe}^{3+} / \text{Fe}^{2+}$ ratio was approximately 3
- Sulphur, which may be either associated with the bentonite or the groundwater (SRB activity in the borehole, see Section 4.1), was found in limited amounts, with 80 at.% attributed to sulphide and 20 at.% attributed to sulphate.

Table 1. XPS results for a carbon steel base metal coupon, at three points on the surface. Etching to 3.3 nm with Ar⁺ ion bombardment was conducted at Point 3.

	Element concentration (normalized at.%) and XPS peak used for quantification								
Point	Fe 2p	O 1s	C 1s	Mg 1s	Na 1s	Ca 2p	S 2p	Al 2p	Si 2p
1	15.5	52.3	27.1	1.6	1.3	1.5	0.7	-	-
2	9.9	51.8	17.2	1.5	1.8	1.3	0.4	7.6	8.5
3 (surface)	13.6	54.0	26.6	1.0	0.8	1.8	2.3	-	-
3 (3.3 nm)	24.0	60.3	8.6	2.0	0.4	3.2	1.6	-	-

Table 2 presents the surface elemental concentrations obtained by XPS analysis from three points for a cold-sprayed copper coupon. The last point (Point 3) was also analysed after ion bombardment. The following observations can be made on the basis of the analysis:

- Similar to steel, a high level of adventitious carbon was identified on the copper surface, as well as elements originating from the bentonite and/or porewater. However, the Si signal was relatively high in all areas (5-11 at.%), while no Al was detected. Sulphur was also found in very limited amounts primarily as sulphide.
- Before ion bombardment, the overall copper signal was low (4-8 at.%), while after ion bombardment, the copper signal was 20 at.%. An atomic ratio for Cu:O of 0.4:1 was found after removal of the adventitious carbon by argon ion bombardment, compared to a ratio of 2:1 for cuprite (Cu₂O), or 1:1 for copper (II) oxide (CuO), suggesting an additional oxygen source that may have originated in the borehole water and/or the bentonite [19]. Deconvolution of the Cu peak indicated that Cu was primarily associated with metallic copper with potentially small amount of Cu₂O.

Table 2. XPS results for cold-sprayed copper coupon, taken over three points on the surface.

Etching to 3.3 nm with Ar⁺ ions was conducted at Point 3.

	Elemental concentration (normalised at.%) and XPS peak used for quantification							
Point	C 1s	O 1s	Cu 2p3	S 2p	Si 2p	Na 1s	Ca 2p	Mg 1s
1	45.4	40.0	7.5	1.3	4.4	0.7	0.7	-
2	36.7	45.4	4.5	-	11.1	1.0	1.3	-
3 (surface)	36.0	45.9	3.7	-	10.4	0.9	1.4	1.7
3 (3.3 nm)	13.2	50.3	20.5	3.0	8.5	-	2.2	2.3

3.2 Characterisation of cross-sections through metal-bentonite interface

Optical and SEM images and EDX analysis results of cross-sectioned coupons are presented in Figures 5 (carbon steel base metal) and 6 (cold-sprayed copper).

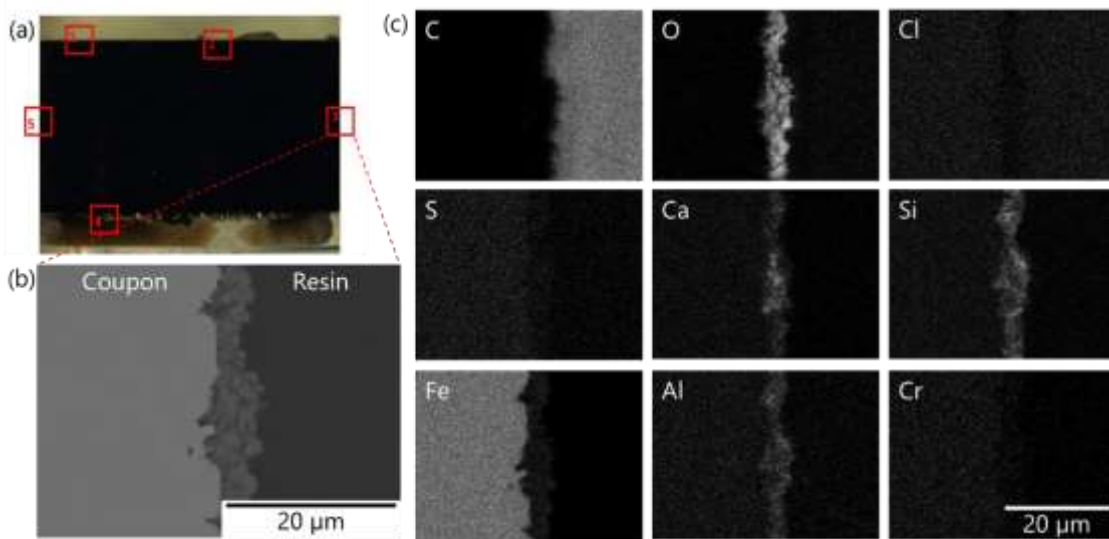


Figure 5. (a) Optical image of cross-section of carbon steel base metal coupon after in situ exposure for 1024 days in pellet bentonite (density = 1450 kg m^{-3}) at the Mont Terri URL. (b) SEM image of coupon-resin interface in area 3 in (a). (c) EDX maps of (b), indicating concentrations of labelled elements.

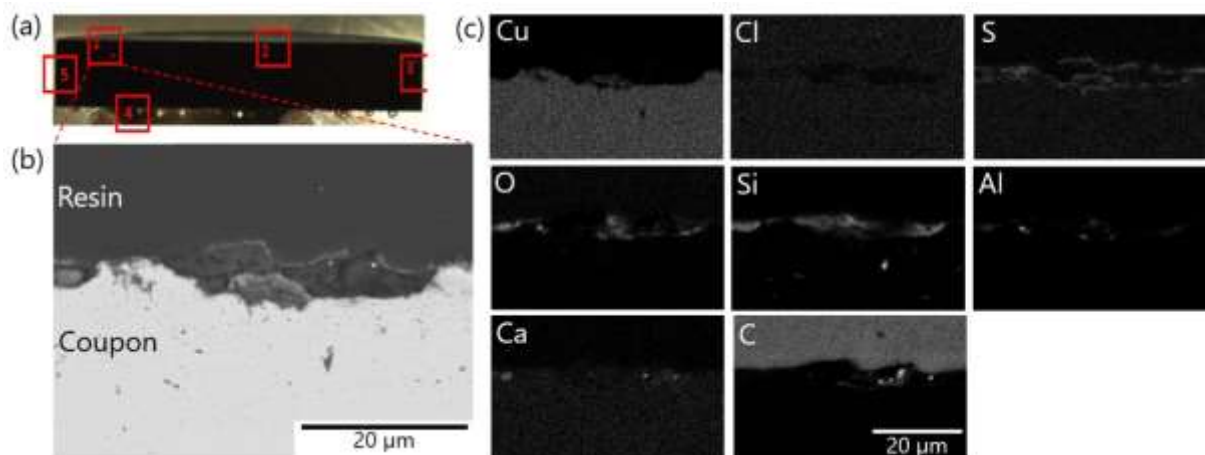


Figure 6. (a) optical image of cross-section of cold-sprayed copper coupon after in situ exposure for 1024 days in pellet bentonite (density = 1450 kg m^{-3}) at the Mont Terri URL and mounted in resin. (b) SEM image of coupon-resin interface in area 1 in (a). (c) EDX maps of (b), indicating concentrations of labelled elements.

The main observations from the analysis for the carbon steel base metal specimen were as follows:

- Components associated with the bentonite (Si, Ca, Al, O) were measured in a surface region, possibly consistent with adhering bentonite.
- Although faint, an Fe signal was measured in this area, suggesting that this region was affected by a corrosion process (e.g. bentonite containing Fe).
- Based on the thickness of the alteration layer adherent to the coupon was at least 1-5 μm thick (some of the alteration products may have been adherent to the bentonite).

For the cold-sprayed copper coupon (Figure 6), the following observations were made:

- The interfacial region was concentrated in silicon, oxygen and, to an extent, sulphur, possibly consistent with adhering bentonite.
- Small amounts of aluminium were detected in Al/O-rich spots possibly associated with the surface preparation process, alumina grit blasting.
- Sulphur was also detected at the interface with the coupon. In some areas, indications that some reaction with the copper may have occurred exist, but in general, there was no clear evidence of a defined corrosion product layer (i.e. a Cu-containing oxide or sulphur compound).

3.3 Corrosion rate

The results of the weight loss measurements are shown graphically in Figures 7 and 8 for carbon steel and copper, respectively. The average corrosion rates of carbon steel samples were about 1-2 $\mu\text{m year}^{-1}$, compared with rates of copper of about 0.02-0.2 $\mu\text{m year}^{-1}$. The average corrosion rates observed on welded carbon steel samples were slightly higher than those observed on bare carbon steel, in agreement with previous analyses [18]. On the contrary, very small or no differences in average corrosion rates were found between different types of copper coupons. Interestingly, the average corrosion rates of both carbon steel and copper coupons were higher in bentonite pellets than in compacted bentonite blocks independent of block density, no differences were observed between the coupons from compacted bentonite blocks with different densities (1550 kg m^{-3} and 1450 kg m^{-3}).

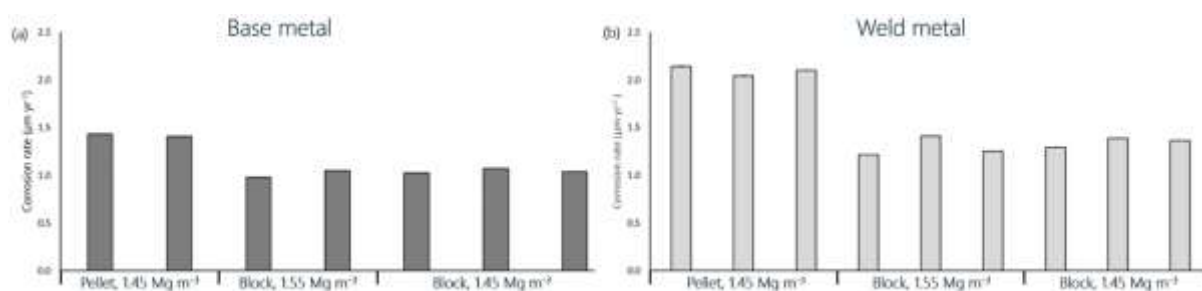


Figure 7. Average corrosion rates for carbon steel base metal (a) and weld metal coupons (b) after an exposure period of 1024 days.

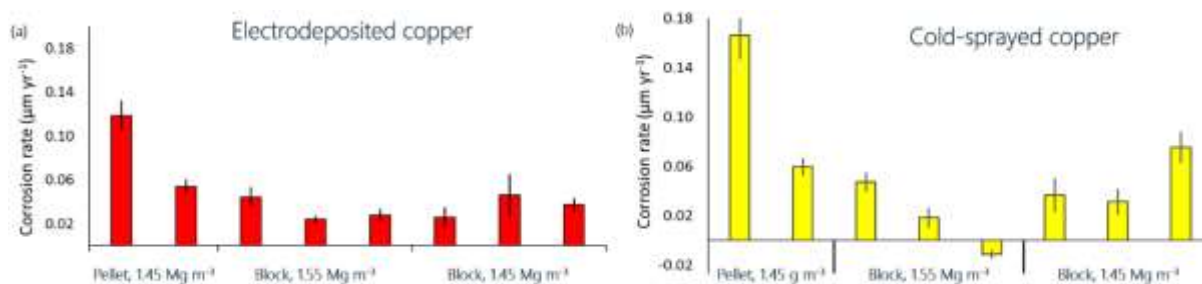


Figure 8. Average corrosion rates for electrodeposited copper coupons (a) and cold-spay copper coupons (b) after an exposure period of 1024 days.

3.4 Profilometry

Average roughness values (R_a) for pristine and exposed coupons are shown in Figure 9. No significant difference in surface roughness before and after exposure were found for base metal carbon steel and cold sprayed copper. On the other hand, welded carbon steel exhibited a slight increase in roughness, while electrodeposited copper exhibited a slight decrease in roughness after exposure.

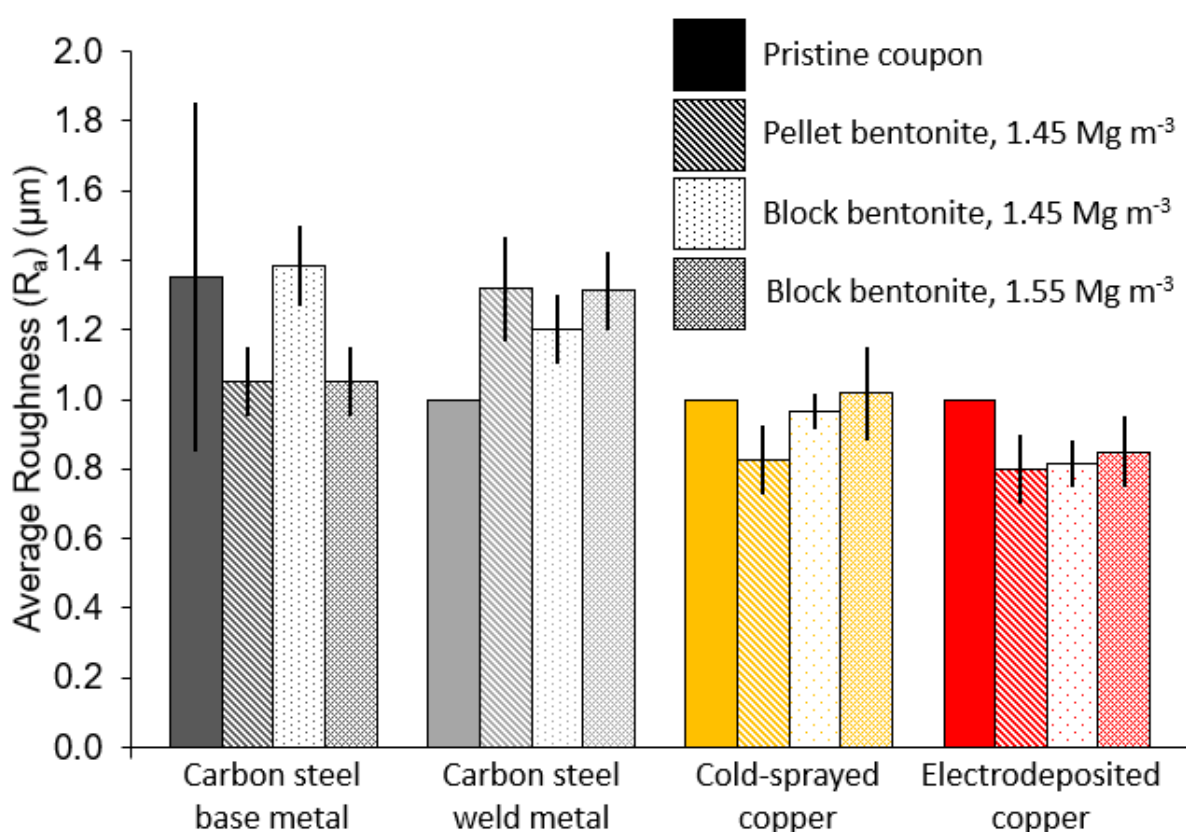


Figure 9. Average R_a values for pristine coupons, and coupons exposed for a nominal duration of 1024 days. Values averaged across 10 independent line profiles.

3.5 Analysis of bentonite

SEM-EDX elemental maps of the bentonite-coupon interface for carbon steel base metal and cold-sprayed copper are given in Figure 11 and Figure 12, respectively.

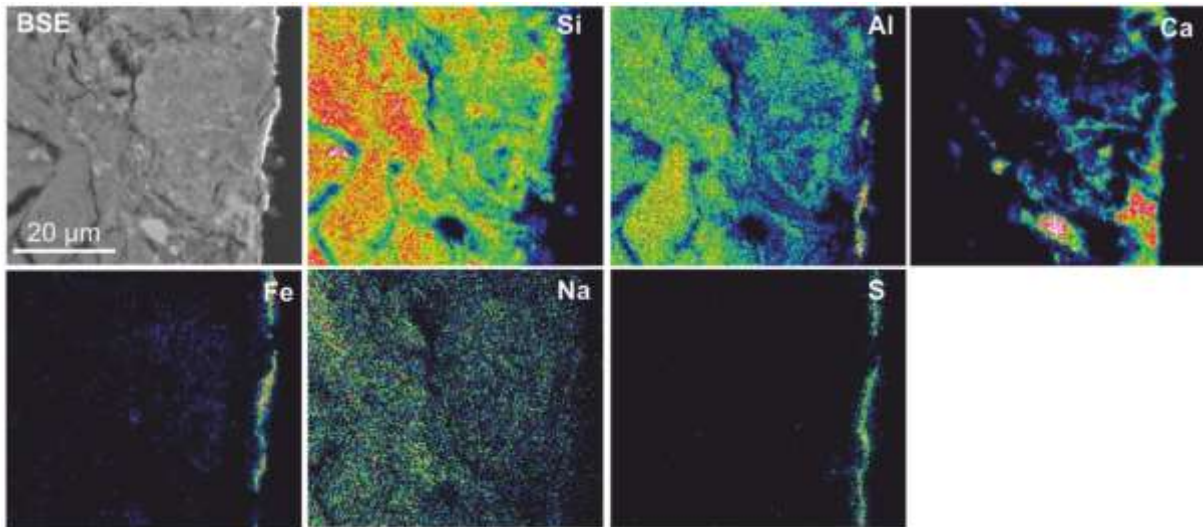


Figure 10. SEM-BSE and EDX elemental maps of the bentonite at the interface with carbon steel base metal after in situ exposure for 1024 days (pellet bentonite density 1450 kg m^{-3}).

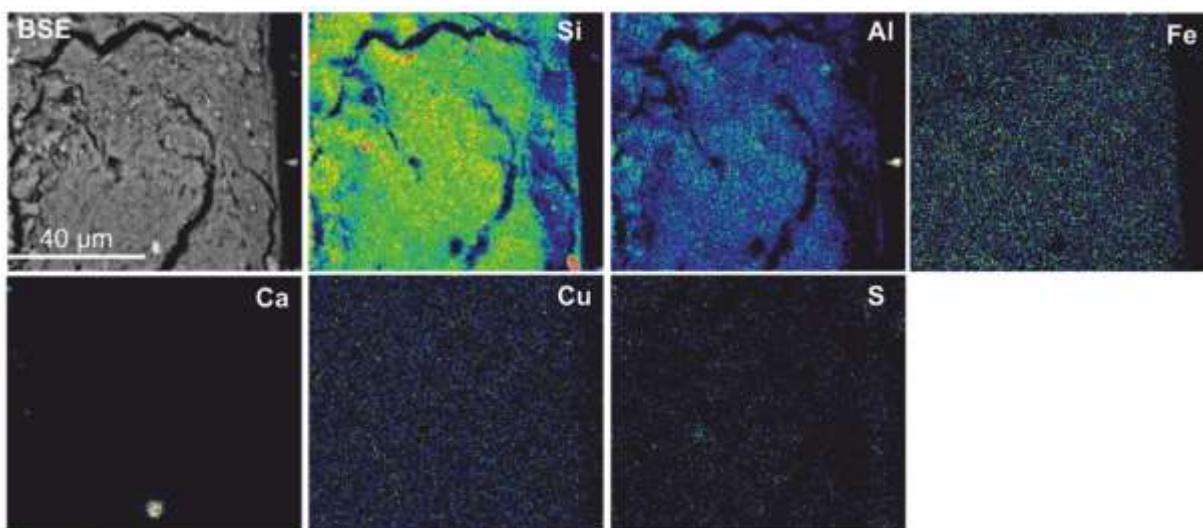


Figure 11. SEM-BSE and EDX elemental maps of the bentonite at the interface with cold-sprayed copper after in situ exposure for 1024 days (pellet bentonite density 1450 kg m^{-3}).

Figure 10 indicates that iron and sulphur were present along the interface between the bentonite and the carbon steel base metal coupon. The concentration of aluminium is increased close to the metal, although the use of alumina particles during surface preparation makes the origin of Al in this region more uncertain. Enrichment in calcium was found in an area $\sim 50 \mu\text{m}$ thick close to the coupon. Further SEM analysis (not shown) revealed a difference in texture within $\sim 2 \text{ mm}$ of the interface, where the bentonite appears to be relatively densely-compacted, with radial microfractures. These only appear to penetrate the bentonite matrix to a similar depth as the visible brown-stained halo (i.e. $\sim 2 \text{ mm}$) and were not present in bentonite samples taken further away from the coupon. It is currently not clear if these microfractures formed during exposure or are an experimental artefact due to the drying of the sample for analysis. XRD showed no evidence of major mineralogical alteration of the bentonite. Evidence of Fe in microfractures close to the coupon were not observed, in contrast with what found in an identical experiment performed in granite host rock [16].

In the bentonite surrounding the cold-sprayed copper coupon (Figure 11), all elements showed typical distributions expected for bentonite; no copper, sulphur or calcium enrichment was detected. In this case no microfractures were detected nor was there any evidence of mineralogical alteration of the bentonite.

4 Discussion

4.1 Carbon Steel

Both Raman and XPS analyses indicated the presence of both magnetite and haematite as corrosion products on the surface of the coupons. Deconvolution of the XPS iron peak exhibited an excess of Fe^{2+} before ion bombardment (excluding pyrite), which may be soluble corrosion products in the adherent bentonite. After ion bombardment the $\text{Fe}^{3+} / \text{Fe}^{2+}$ ratio increased to values of about 3, more consistent with a magnetite-haematite mixture. SEM-EDX analysis of cross-sectioned base metal steel coupons show that the alteration layer (taken to be the area containing Fe in the O-, Al- and Ca-rich region found on the surface) was at least $\sim 1\text{-}5\ \mu\text{m}$ thick (a portion of the layer may remain attached to the bentonite during the removal of the coupon). These values are similar to values estimated through weight loss measurements. Specifically, after 2.8 years of exposure, an average corrosion rate of about $1\text{-}1.5\ \mu\text{m yr}^{-1}$ was calculated for this material (see Figure 7). Assuming a pure magnetite corrosion product layer with a Pilling-Bedworth ratio of 2.1, this is equivalent to a corrosion product layer thickness of approximately $8.3\ \mu\text{m}$. The fact that the observed layer thickness was somewhat less than that estimated by weight loss measurements, suggests that some of the corrosion product remained attached to the bentonite and/or that a significant fraction of the iron released during corrosion did not precipitate at the coupon-bentonite interface, rather underwent migration further into the bentonite. Interestingly, iron-stained bentonite was seen to extend approximately 2 mm from the coupon surface (Figure 1). If iron was distributed over such a thickness this would mean that, microscopically, the iron was finely distributed (possibly as nanoparticulate) and below the resolution of the analytical techniques applied.

The enrichment of calcium in an area a few 10s of μm thick next to the steel surface, as seen in Figures 5 and 11, has been systematically reported before [18, 29, 30, 31]. Since MX-80 bentonite contains Na-montmorillonite and no alteration of the clay was identified in

petrographical analyses, the most probable source of Ca would be accessory minerals such as calcite (0 – 1.3 wt.%) and gypsum (0.7 – 14 wt.%) [32]. The exact mechanism of enrichment is currently unclear, but it can be assumed that local processes related to corrosion at the interface, such as water consumption, hydrogen production, and pH increase due to water reduction, could be responsible for calcite precipitation there.

Figure 13 shows average corrosion rates of base metal carbon steel at different exposure durations. The average corrosion rates decrease at increasing exposure duration, consistent with laboratory experiments in similar conditions [31], which showed a decrease in instantaneous corrosion rate with time over several years, albeit at an elevated temperature of 60 °C. Usually, the fall in corrosion rate is attributed to an increase in the protectiveness of the corrosion product layer developing on carbon steel with time [31]. In addition, the decrease in corrosion rate could be the result of a decrease in the rate of transport of groundwater and/or corrosive reactants through the bentonite, associated with swelling of the bentonite. Although the bentonite was pre-saturated for ten days before emplacement in the borehole, it is possible that swelling processes continued during exposure, at least over an initial period.

Interestingly, comparing the corrosion rates in Figure 13 with measurements of microbial activity in the bentonite (primarily aerobic heterotrophs) and the borehole water surrounding the modules (sulphate reducing bacteria) reported elsewhere [19], shows no correlation between the two. This indicates that microbially-induced corrosion is not a significant contributor to the material loss measured during this experiment.

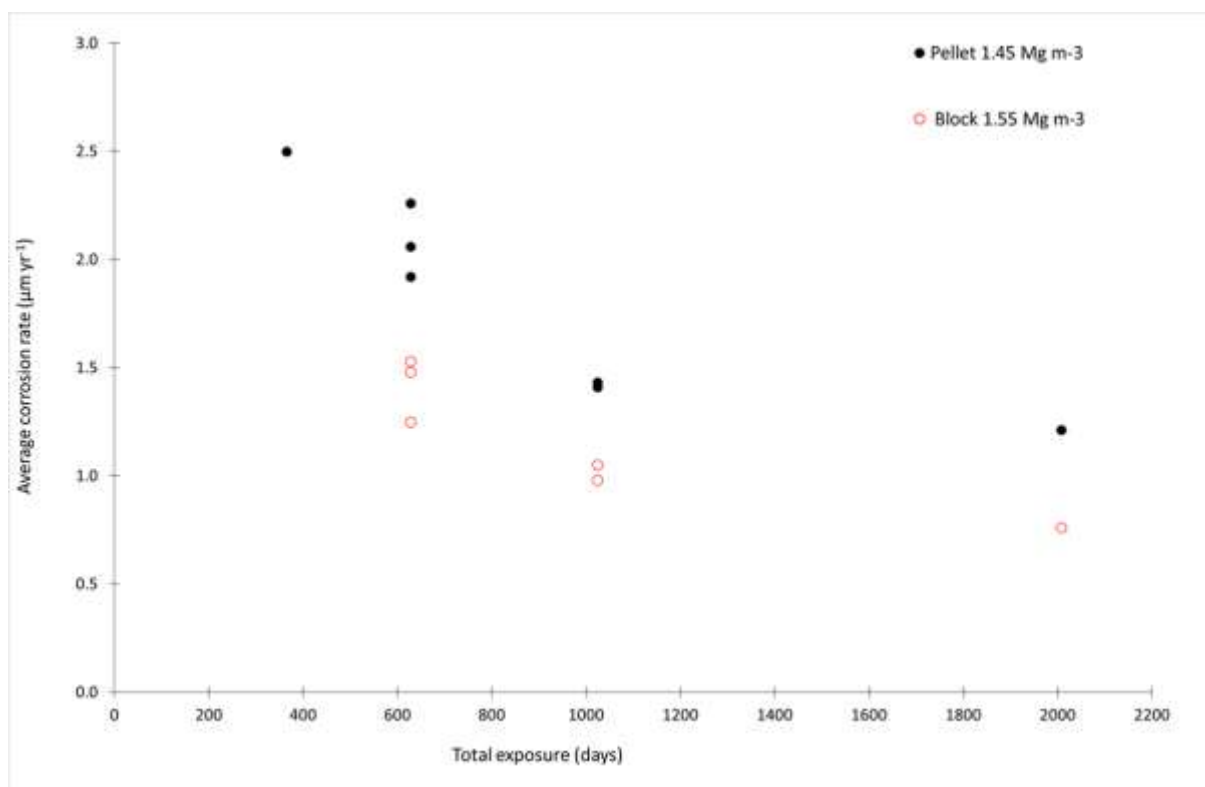


Figure 12. Average corrosion rate for carbon steel base metal coupons in pellet and block bentonite exposed in situ after different exposure times. Data for 1 and 1.5 years are from [18]. Preliminary data for 5.5 years from on-going work are also shown.

Furthermore, the results from Figure 12 indicate that the increased corrosion rates for carbon steel in the pellet bentonite compared to compacted blocks shown in Figure 7, are a systematic occurrence which is independent of the exposure duration. The reason for this is currently uncertain since, in principle, one may expect that the same corrosion behaviour is observed in the same dry density bentonite. A potential explanation could be that the preparation method, i.e. the compaction of blocks under vacuum followed by anoxic packaging and storage, can change a corrosion-relevant property of the bentonite. Potentially important factors could be: (i) the extent of voidage near the surface of the coupons and hence the space available for reactants and reaction products to accumulate; (ii) the transport of water, oxidants and corrosive

species from the groundwater to the corroding surface, which could affect the rate of corrosion, or, (iii) the amount of oxygen initially absorbed in the bentonite.

4.2 Copper

Regarding the identification of a corrosion product layer on copper, different analytical techniques provided conflicting evidence. Raman spectroscopy suggested the presence of CuO and Cu₂O on the surface, although the XPS analysis identified primarily metallic copper with possibly a small amount of Cu₂O. SEM-EDX analysis of cross sections did not identify a defined corrosion product layer on the copper coupons at the copper/bentonite interface. Some sulphur was detected, mainly interspersed close to the copper surface. Similarly, SEM-EDX analysis of the surface showed that the composition of the surface was predominantly copper, with some residual bentonite. Oxygen seemed to be primarily associated with species originating in the bentonite, rather than with copper-rich regions. This would suggest that, if any copper-oxide was present, this would have been much thinner than the SEM penetration depth (< 1 µm). This is in agreement with the measured corrosion rates and the minimal changes in surface roughness.

The average corrosion rates of copper based on weight loss measurements were of the order of 0.02-0.2 $\mu\text{m year}^{-1}$, typically a factor of 10-20 times lower than for carbon steel, with the two types of copper coatings exhibiting similar corrosion rates. The measured corrosion rates are consistent with other in situ experiments carried out in the Swedish disposal programme when an intact, high-density bentonite buffer was used (MiniCan 4) [35, 36]. Copper samples were not included in modules retrieved earlier [18], and so it is not yet possible to draw any conclusions about the effect of time on the corrosion rate or roughness of the copper samples. The enrichment in sulphur at the copper surface was considerably less than the typical extent of alteration observed for the carbon steel coupon surfaces. This is also consistent with the very low average corrosion rate measured through weight loss, if it is assumed that the copper- and sulphur-rich patches are due to the formation of a corrosion product (e.g. a copper sulphide). There were no indications of differences in bentonite density and/or morphology near the metal surface, differently to what was seen in the case of steel. The presence of the corroding copper surface had no effect on the iron content of the octahedral sheet in the montmorillonite and, in general, did not result in any mineralogical alteration of the bentonite, as expected from the fact that there are no structural sites for monovalent cations in the clay mineral.

5 Conclusions

This paper presents results from the analysis of base metal and electron beam welded carbon steel, and cold sprayed and electrodeposited copper coatings exposed within bentonite clay of various forms and densities in an anoxic borehole in Opalinus Clay for a period of ~2.8 years. After retrieval there were signs of widespread heterogeneous alteration on carbon steel coupons and in the surrounding bentonite, but limited signs of reaction on and around copper samples. At the interface between steel and bentonite an alteration layer rich in O, Si, Al, Ca and Fe, at least 1-5 μm thick, was observed in SEM/EDX cross sections. Raman and XPS analyses identified predominantly magnetite (Fe_3O_4), and some hematite (Fe_2O_3). The surface of copper coupons was primarily metallic copper with potentially small amounts of Cu_2O and interspersed sulphide, but the thickness of reaction products (if any) was too low for most analytical techniques. The average corrosion rate of carbon steel during the 1024 day exposure period was ~1-1.5 $\mu\text{m y}^{-1}$ for base metal and 1.5-2 $\mu\text{m y}^{-1}$ for the weld. The average corrosion rates for copper during the 1024 day exposure were ~0.02 – 0.2 $\mu\text{m y}^{-1}$ with both types of coating exhibiting similar rates. Interestingly, it appears that the preparation of bentonite can have an influence on corrosion, as corrosion rates in bentonite pellets were systematically higher than in compacted blocks. On the other hand, no correlation was found between the corrosion rate and the evolution of microbial activity in the bentonite and the surrounding porewater, indicating that MIC is not an important contributor to material loss in compacted bentonite at the densities studied.

6 Acknowledgements

The authors would like to acknowledge TWI (UK) and NWMO (Canada) for the provision of carbon steel and copper coatings respectively, Special Techniques (UK) for the manufacture of test specimens, Colin Johnston (Oxford University Materials Characterisation Service) for

analytical data and useful discussions, Clay Technology (Sweden) for preparing bentonite blocks, and the Mont Terri Consortium and the experimental partners (NWMO, Andra, RWM) for technical and financial support.

7 References

1. R. Patel, C. Punshon, J. Nicholas, P. Bastid, R. Zhou, C. Schneider, N. Bagshaw, D. Howse, E. Hutschison, R. Asano. **2012**. Canister Design Concepts for Disposal of Spent Fuel and High Level Waste. Nagra Technical Report NTB 12-06 . Nagra, Wettingen, Switzerland
2. N. Diomidis, F. King. **2020**. Development of copper coated canisters for the disposal of SF and HLW in Switzerland. Nagra Technical Report NTB 20-01. Nagra, Wettingen, Switzerland.
3. P. G. Keech, S. Ramamurthy, J. Chen, R. Jacklin and D. W. Shoesmith, *Corrosion Engineering, Science and Technology* **2014**, 49, 6
4. Leupin, O. X.; Smith, P.; Marschall, P.; Johnson, L.; Savage, D.; Cloet, V., J. Schneider, R. Senger. **2016**. High-level waste repository-induced effects. Nagra Technischer Bericht NTB 14-13. Nagra, Wettingen, Switzerland
5. Blechschmidt, I. and S. Vomvoris. *In Geological Repository Systems for Safe Disposal of Spent Nuclear Fuels and Radioactive Waste*, 2nd Edition, M.J. Apted and J. Ahn (eds.). Elsevier Woodhead Publishing (Duxford, UK) **2017**., Chap.5.
6. Smart, N., A. Rance, B. Reddy, S. Lydmark, K. Pedersen, and C. Lilja. **2011b**. Further studies of in situ corrosion testing of miniature copper-cast iron nuclear waste canisters. *Corros. Eng. Sci. Tech.*, 46, 142-147.

7. Smart, N.R., A.P. Rance, B. Reddy, L. Hallbeck, K. Pedersen, and A.J. Johansson. **2014**. In situ evaluation of model copper-cast iron canisters for spent nuclear fuel: a case of microbiologically influence corrosion (MIC). *Corros. Eng. Sci. Tech.*, 49, 548-553.
8. Schlegel, M.L., S. Necib, S. Daumas, C. Blanc, E. Foy, N. Trcera, and A. Romaine. **2016**. Microstructural characterisation of carbon steel corrosion in clay borehole water under anoxic and transient acidic conditions. *Corros. Sci.*, 109, 126-144
9. Schlegel, M.L., S. Necib, S. Daumas, M. Labat, C. Blanc, E. Foy, and Y. Linard. **2018**. Corrosion of the carbon steel-clay borehole water interface under anoxic alkaline and fluctuating temperature conditions. *Corros. Sci.*, 136, 70-90
10. Necib, S., Y. Linard, D. Crusset, N. Michau, S. Daumas, E. Burger, A. Romaine, and M.L. Schlegel. **2016a**. Corrosion at the carbon steel-clay borehole water and gas interfaces at 85 °C under anoxic and transient acidic conditions. *Corros. Sci.*, 111, 242-258.
11. Necib, S., C. Bataillon, S. Daumas, M.L. Schlegel, and D. Crusset. **2016b**. Corrosion processes and microbial activity of carbon steel in the context of geological repository in clay environment. *MRS Advances*, 1, 4185-4191.
12. Necib, S., Y. Linard, D. Crusset, M. Schlegel, S. Daumas, and N. Michau. **2017a**. Corrosion processes of C-steel in long-term repository conditions. *Corros. Eng. Sci. Tech.*, 52:Sup1, 127-130.
13. Necib, S., Y. Linard, A. Bellefleur, M. Schlegel and S. Daumas. **2017b**. Corrosion of metallic materials in compacted Callovo-Oxfordian claystone at 50 °C. In *Proceedings of Eurocorr 2017, European Federation of Corrosion*.
14. Necib, S., N. Diomidis, P. Keech, M. Nakayama. **2017c**. Corrosion of carbon steel in clay environments relevant to radioactive waste geological disposals, Mont Terri rock laboratory (Switzerland). *Swiss J. Geosci.*, 110, 329-342.

15. Madina, V. **2016**. Corrosion study of FEBEX-DP components. Nagra Working Report NAB 16-54.
16. B. Reddy, C. Padovani, A. Cook, N.R. Smart¹, A.P Rance, A. Milodowski, L. Field, S. Kemp, A. Martin, N. Diomidis, presented at the 7th. International Workshop on Long-Term Prediction of Corrosion Damage in Nuclear Waste Systems, Nancy, France **2019**.
17. Van Iseghem, P. B. Kursten, E. Valcke, H. Serra, J. Fays and A. Sneyers. **2003**. In situ testing of waste forms and container materials: contribution to the identification of their long term behaviour. In D. Féron and D.D. Macdonald (Eds.), Prediction of long term corrosion behaviour on nuclear waste systems, European Federation of Corrosion Publications Number 36 (Maney Publishing), 35-48.
18. N.R. Smart, B. Reddy, A. P. Rance, D. J. Nixon, M. Frutschi, R. Bernier-Latmani, N. Diomidis, *Corrosion Engineering, Science and Technology* **2017**, 52:sup1, 101-112.
19. N. Burzan, R. Bernier-Latmani, N. Diomidis. 2020. Temporal evolution of the microbial community associated with Wyoming bentonite MX-80 saturated with Opalinus Clay rock porewater in situ. In preparation.
20. P. Keech, P. Lin, N. Mahalanobis, Electrodeposited Copper Coatings for Used Fuel Containers, *35th Annual Conference of Canadian Nuclear Society*, May, **2015**.
21. P. Keech, P. Vo, D. Poirier J.G. Legoux, Cold Spray Copper Coatings for Used Fuel Containers, *35th Annual Conference of Canadian Nuclear Society*, May, **2015**.
22. ASTM G1-03(2017), *Standard Practice for Preparing, Cleaning, and Evaluating Corrosion Test Specimens*, ASTM International, West Conshohocken, PA, **2017**.
23. N. Diomidis, B. Reddy, R. Bernier-Latmani. 2020. Corrosion of carbon steel in anaerobic saturated bentonite: in situ and ex situ experiments. Part 1. Nagra Arbeitsbericht NAB 20-10. Nagra, Wettingen, Switzerland.

24. O.N.Shebanova and P.Lazor, , *Journal of Raman Spectroscopy*, **2003**; 34; 845-852
25. M. Hanesch, *Geophysical Journal International* 2009, 177(3), 941-948.
26. M.R. Nuys, *Characterization and Modification of Copper and Iron Oxide, Energy and environment* **2015**, ISBN 978-3-95806-096-8, 291.
27. M. Davies and P.J.B. Scott, *Oilfield Water Technology, NACE International*, **2006**, 280.
28. J.W. Mullin, *Crystallization*, 4th Edition, Elsevier, **2001**
29. A.E. Milodowski, M.R. Cave, S.J. Kemp, H. Taylor, B. Vickers, K. Green, C.L. Williams and R.A. Shaw, Mineralogical Investigations of the Interaction Between Iron Corrosion Products and Bentonite from the NF-PRO Experiments (Phase 1), SKB Technical Report TR-09-02, **2009**.
30. A.E. Milodowski, M.R. Cave, S.J. Kemp, H. Taylor, K. Green, C.L. Williams and R.A. Shaw, Mineralogical Investigations of the Interaction Between Iron Corrosion Products and Bentonite from the NFPRO Experiments (Phase 2), SKB Technical Report TR-09-03, **2009**.
31. N. R. Smart, B. Reddy, A. P. Rance, D. J. Nixon and N. Diomidis, *Corrosion Engineering, Science and Technology*, **2017**.52:sup1, 113-126
32. A. Jenni, P. Wersin, T. Thoenen, B. Baeyens, A. Ferrari, T. Gimmi, U. Mäder, P. Marschall, W. Hummel & O. Leupin. **2019**. Bentonite backfill performance in a high-level waste repository: a geochemical perspective. Nagra Technical Report NTB 19-03. Nagra, Wettingen, Switzerland.

33. N. Burzan, R. Bernier-Latmani, N. Diomidis. 2020. Temporal evolution of the microbial community associated with Wyoming bentonite MX-80 saturated with Opalinus Clay rock porewater in situ. In preparation.
34. C. Padovani, F. King, C. Lilja, D. Féron, S. Necib, D. Crusset, V. Deydier, N. Diomidis, R. Gaggiano, T. Ahn, P.G. Keech, D.D. Macdonald, H. Asano, N. Smart, D.S. Hall, H. Hänninen, D. Engelberg, J.J. Noël, D.W. Shoesmith, *Corrosion Engineering, Science and Technology*, **2017**, 52, - Issue supl
35. A. Gordon, L. Sjögren, C. Taxén, A.J. Johansson, “Retrieval and post-test examination of packages 4 and 5 of the MiniCan field experiment”, SKB report TR-16-12 (2017).
36. C. Padovani, B. Reddy, A. Rance, N. Smart, S. Swanton, J. Schofield, A. Milodowski, L. Field, S.J. Kemp, N. Diomidis, A. Martin, A. J. Johansson, R.J. Winsley, M. Cowley, Progress in demonstrating the performance of Engineered Barriers for the disposal of HLW and SNF: lab studies and demonstration experiments, proceedings of WM2020 Conference, March 8 – 12, 2020, Phoenix, Arizona, USA